HHS Public Access

Author manuscript

Free Radic Biol Med. Author manuscript; available in PMC 2016 December 01.

Published in final edited form as:

Free Radic Biol Med. 2015 December ; 89: 369–378. doi:10.1016/j.freeradbiomed.2015.08.015.

Fluoride induces oxidative damage and SIRT1/autophagy through ROS-mediated JNK signaling

Maiko Suzuki, **Cheryl Bandoski**, and **John D. Bartlett***

Department of Mineralized Tissue Biology, The Forsyth Institute & Harvard School of Dental Medicine, 245 First Street, Cambridge, MA

Abstract

Fluoride is an effective caries prophylactic, but at high doses can also be an environmental health hazard. Acute or chronic exposure to high fluoride doses can result in dental enamel and skeletal and soft tissue fluorosis. Dental fluorosis is manifested as mottled, discolored, porous enamel that is susceptible to dental caries. Fluoride induces cell stress, including endoplasmic reticulum stress and oxidative stress, which leads to impairment of ameloblasts responsible for dental enamel formation. Recently we reported that fluoride activates SIRT1 and autophagy as an adaptive response to protect cells from stress. However, it still remains unclear how SIRT1/autophagy is regulated in dental fluorosis. In this study, we demonstrate that fluoride exposure generates reactive oxygen species (ROS) and the resulting oxidative damage is counteracted by SIRT1/autophagy induction through c-Jun N-terminal kinase (JNK) signaling in ameloblasts. In the mouse-ameloblast-derived cell line LS8, fluoride induced ROS, mitochondrial damage including cytochrome-c release, up-regulation of UCP2, attenuation of ATP synthesis, and H2AX phosphorylation (γH2AX), which is a marker of DNA damage. We evaluated the effects of the ROS inhibitor N-acetylcysteine (NAC) and the JNK inhibitor SP600125 on fluoride-induced SIRT1/autophagy activation. NAC decreased fluoride-induced ROS generation and attenuated JNK and c-Jun phosphorylation. NAC decreased SIRT1 phosphorylation and formation of the autophagy marker LC3II, which resulted in an increase in the apoptosis mediators γH2AX and cleaved/activated caspase-3. SP600125 attenuated fluoride-induced SIRT1 phosphorylation, indicating that fluoride activates SIRT1/autophagy via the ROS-mediated JNK pathway. In enamel organs from rats or mice treated with 50, 100, or 125 ppm fluoride for 6 weeks, cytochrome-c release and the DNA damage markers 8-oxoguanine, p-ATM, and γH2AX were increased compared to those in controls (0 ppm fluoride). These results suggest that fluoride-induced ROS generation causes mitochondrial damage and DNA damage, which may lead to impairment of ameloblast function. To counteract this impairment, SIRT1/autophagy is induced via JNK signaling to protect cells/ameloblasts from fluoride-induced oxidative damage that may cause dental fluorosis.

*Corresponding author. Fax: +(617)8928510. jbartlett@forsyth.org (J.D. Bartlett).

Conflicts of Interest

None.

Keywords

Fluorosis; Ameloblast; ROS; Oxidative damage; JNK; Sirtuin; Autophagy

1. Introduction

Fluoride is a naturally occurring mineral that protects against tooth decay. The Centers for Disease Control and Prevention (CDC) recommends public water fluoridation at an optimal fluoride concentration of 0.7 ppm in order to prevent dental caries [1]. However, acute or chronic fluoride overexposure can result in enamel [2] and skeletal fluorosis [3], renal toxicity [4], epithelial lung cell toxicity [5], and reproductive toxicity [6, 7]. Dental fluorosis is a developmental disorder caused by fluoride exposure during enamel formation, which manifests as mottled, discolored, and porous enamel [8]. Over the last decade, concerns have arisen about the prevalence of fluorosis around the world, including the United States, India, and China [9]. Recent reports indicate that in the United States the prevalence of mild to severe dental fluorosis among children aged 6–11 is 33.4% and in adolescents aged 12–15 it is 40.6% [10].

Ameloblasts are enamel organ cells that are responsible for enamel formation. Ameloblasts occur as single layers of cells located directly adjacent to the forming enamel. Enamel development occurs in stages as defined by the morphology of the ameloblasts [11]. During the secretory stage, tall columnar ameloblasts secrete proteins into the enamel matrix. During the maturation stage, as the enamel begins to harden into its final form, the ameloblasts shorten and reabsorb the secreted proteins. Most of the mineral precipitates in the maturation stage, which generates abundant hydrogen ions, causing ameloblasts to be exposed to an acid environment ($pH < 6.0$) [12]. Acid promotes the conversion of fluoride into highly toxic HF that can easily penetrate the cell membrane. We have shown that acid increases fluoride toxicity and that the acid environment of the maturation stage makes ameloblasts more susceptible to the toxic effects of fluoride exposure [13]. Specifically, fluoride decreases mRNA expression of the maturation-stage-specific genes (*Klk4* and *Amtn*) in vivo. However, since the secretory stage remains at neutral pH, fluoride had little to no effect on mRNA expression levels of secretory-stage-specific genes (*Ambn*, *Amel*, *Enam*, and *Mmp20*).

Fluoride exerts diverse cellular effects in a dose-, cell-type-, and tissue-dependent manner. We and others have shown in several tissues, including the enamel organ, that high-dose fluoride causes cell stress, such as endoplasmic reticulum (ER) stress [14–16] and oxidative stress [7,17]. Fluoride exposure increases the generation of superoxide (O_2^-) and other reactive oxygen species (ROS) that are associated with fluoride toxicity [18,19]. Low and intermediate levels of ROS are physiologically important as cell signaling molecules, whereas high ROS concentrations that preclude cell clearance cause oxidative stress, mitochondrial dysfunction, and cellular and DNA damage that can result in cell death. ROS induces uncoupling protein 2 (*Ucp2*), which is an antioxidant and belongs to the mitochondrial anion transporter superfamily located in the inner mitochondrial membrane. UCP2 negatively regulates mitochondrial membrane potential and ATP synthesis to

decrease mitochondrial superoxide production when cells experience oxidative stress [20]. ROS can cause DNA double strand breaks (DSB) and phosphorylation of histone H2AX (γH2AX), which is a DNA damage biomarker that accumulates within seconds following induction of a DSB. This phosphorylated histone can extend over tens of kilobases of DNA flanking the break site and plays a role in the amplification of the DNA damage response signaling cascade [21,22]. H2AX is phosphorylated by c-Jun N-terminal kinase (JNK) signaling and its phosphorylation is required for caspase-induced DNA fragmentation [23]. Previously we demonstrated that fluoride increases *Ucp2* expression in rat enamel organ (EO) [17] and induces DNA fragmentation in LS8 cells [15]. However, the mechanism underlying oxidative damage, including mitochondrial dysfunction and DNA damage caused by fluoride exposure in dental fluorosis, remains unknown.

Recently we reported that fluoride activates SIRT1 and autophagy as an adaptive response to protect cells from cell stress [24]. Sirtuins (SIRT1–SIRT7) are a family of highly conserved NAD^+-dependent class III histone deacetylases (class III HDACs). SIRT1 is the mammalian homolog of yeast silent information regulator-2 (Sir2), which is the most widely studied of the sirtuins [25–27]. SIRT1 expression increases under various physiological conditions, including nutrient starvation, aging, and cell stress such as oxidative stress [28–30]. During cell stress, SIRT1 is regulated by various factors [31]. For example, transcription factors including peroxisome-proliferator-activated receptors (PPARs) [32,33] and cAMP response element binding (CREB) [34] enhance SIRT1 expression. Activation of c-Jun N-terminal kinase (JNK) by ROS results in SIRT1 phosphorylation [35], and subsequently SIRT1 deacetylates histone and nonhistone proteins [30,36]. In addition to JNK signaling, ROS activates AMP-activated protein kinase (AMPK) to enhance SIRT1 activity by increasing cellular NAD^+ levels [37]. SIRT1 regulates several biological events including autophagy, cell metabolism, longevity, apoptosis, and DNA repair (reviewed in [31]). However, the mechanism of SIRT1/autophagy regulation in dental fluorosis is unclear.

Understanding how fluoride-induced oxidative stress contributes to the pathogenesis of dental fluorosis and how fluoride-induced oxidative stress plays a critical role in SIRT1/autophagy will allow us to better understand the pathophysiology of dental fluorosis. Therefore, the aim of the present study is to evaluate fluoride-induced oxidative damage in ameloblasts and determine the role of ROS in fluoride-induced cytotoxicity and the adaptive response (induction of SIRT1 and autophagy) in dental fluorosis. In the present study, we demonstrate that fluoride-induced ROS generation leads to mitochondrial dysfunction and DNA damage in ameloblasts. On the other hand, ROS generation was required for fluoride-induced JNK signaling to activate SIRT1 and autophagy as an adaptive response. These results suggest that fluoride-induced oxidative damage can lead to impairment of ameloblast function, while simultaneously playing a pivotal role in the induction of the adaptive response to mitigate cytotoxicity in dental fluorosis.

2. Materials and methods

2.1. Animals

The rodent model is a valuable tool for studying enamel formation in mammals. Since rodent incisors erupt continuously, every stage of enamel development is present along the

length of the rodent incisor. The incisors are categorized as mandibular or maxillary and their respective enamel organs may be segregated into the secretory stage and the maturation stage of enamel development. Sprague–Dawley rats (6-week-old) and C57BL/6 mice (6-week-old) were purchased from Charles River Laboratories (Wilmington, MA) and were provided water containing 0, 50, 100, or 125 ppm fluoride as sodium fluoride (NaF) ad libitum. After 6 weeks, animals were euthanized and incisors were extracted for immunohistochemical procedures or real-time PCR analysis. All animals were treated humanely and all handling procedures were approved by the Institutional Animal Care Use Committee (IACUC) at the Forsyth Institute. The Forsyth Institute is accredited by the Association for Assessment and Accreditation of Laboratory Animal Care International (AAALAC) and follows the *Guide for the Care and Use of Laboratory Animals* (NRC1996).

2.2. Cell culture

The mouse-ameloblast-derived cell line (LS8) [38] was maintained in alpha minimal essential medium with GlutaMAX (Life Technologies, Grand Island, NY) supplemented with fetal bovine serum (10%) and sodium pyruvate (1 mM). Cells were treated with sodium fluoride (NaF) with/without N-acetylcysteine (NAC) or SP600125 as indicated. NaF and NAC were obtained from Fisher Scientific (Pittsburgh, PA). The JNK inhibitor SP600125 was purchased from Calbiochem (Billerica, MA). GKT137831 (NOX1/NOX4 inhibitor, Selleckchem Houston, TX) and 5Z-7-oxozealenol (TAK1 inhibitor, Tocris Bioscience, Bristol, UK) were used at the indicated concentrations.

2.3. Reactive oxygen species measurements

Intracellular ROS production was measured with a cell-per-meant indicator for ROS, chloromethyl (CM)-H_2DCFDA (2′,7′-dichlorodihydro fluorescein diacetate) (#C6827; Invitrogen, Carlsbad, CA). Briefly, 5×10^4 LS8 cells were cultured in 96-well plates overnight. The cells were then treated with NaF at the indicated concentrations, or left untreated, for 3 h. Cells were washed with sterile PBS and 100 μl serum-free culture media was added, which contained 5 μM CM-H_2DCFDA. Cells were incubated at 37 °C for 30 min followed by washing and addition of 100 μl PBS per well. ROS concentrations were determined by fluorescence measurements (485/520 nm).

2.4. Western blot analysis

Depending on the experiment, LS8 cells were treated with 0–5 mM NaF. Total proteins were extracted with Lysis buffer (25 mM Tris · HCl pH7.4, 150 mM NaCl, 1% NP-40, 1 mM EDTA, 5% glycerol) containing protease inhibitor cocktail (Thermo Scientific, Rockford, IL). Nuclear proteins were isolated using a nuclear extract kit (Active Motif, Carlsbad, CA). Mitochondrial fractions and cytosolic fractions were isolated using a mitochondria isolation kit for cultured cells (Thermo Scientific). Equal amounts of protein per lane (5–20 μg) were loaded onto Mini-Protean TGX gels (Biorad, Hercules, CA), transferred to Trans-Blot Turbo Transfer nitrocellulose membranes (Biorad), and probed with primary antibodies. Primary antibodies included rabbit anti-cytochrome-c, rabbit anti-VDAC1/Porin, rabbit anti-UCP2, (Abcam, Inc., Cambridge, MA), rabbit anti-p-SIRT1

[Ser47] (Bioss, Inc., Woburn, MA), rabbit anti-γH2AX [Ser139], rabbit anti-SIRT1, rabbit anti-LC3, rabbit anti-p-JNK [Thr183/Tyr185], rabbit anti-JNK, rabbit anti-p-c-Jun [Ser63], rabbit anti-c-Jun, rabbit anti-α-tubulin, and rabbit anti-histone H3 (Cell Signaling Technology, Danvers, MA). The secondary antibody was HRP-conjugated goat anti-rabbit IgG (Biorad). Enhanced chemiluminescence was performed with SuperSignal West Pico (Thermo Scientific), and bands were quantified by densitometry using Quantity One software (Biorad). Each western blot was performed a total of three to four times.

2.5. Intracellular ATP measurements

ATP levels in LS8 cells were measured using an ATP assay kit (Abcam), which utilizes the phosphorylation of glycerol to generate a product that is quantified by colorimetric means (570 nm). LS8 cells were treated with 0, 5, or 10 mM NaF for 6 h and ATP was measured according to the manufacturer's instructions. OD at 570 nm was measured in a microplate reader and ATP concentrations were calculated by use of a standard curve.

2.6. Immunohistochemistry/immunofluorescence

Immunohistochemistry was performed as described previously [15]. Briefly, rat or mouse incisors were extracted after 6 weeks fluoride treatment and fixed in paraformaldehyde, demineralized with EDTA for 2 weeks, and embedded in paraffin. Sections were incubated with primary antibodies: rabbit anti-cytochrome-c, mouse anti-8-oxoguanine, rabbit anti-p-JNK [phospho T183/Y185] (Abcam), rabbit anti-γH2AX, and rabbit anti-p-ATM (Sigma-Aldrich Co., St. Louis, MO), followed by incubation with a peroxidase-conjugated secondary antibody, Vectastain Elite ABC Regent (Vector Labs, Burlingame, CA), and ImmPACT DAB kit (Vector Labs). Sections were counterstained with 0.1% Fast Green in PBS and examined by light microscopy.

For immunofluorescence staining, paraffin sections were quenched of endogenous autofluorescence with 2% $NaBH_4$ in PBS. Nonspecific antibody binding was blocked by incubating with PBS containing 1.5% goat serum. The slides were then sequentially incubated, starting with primary antibodies diluted in PBS containing 1% BSA incubated overnight at 4 °C, followed by addition of fluorescent-labeled secondary antibodies for 1 h at room temperature. The primary antibodies were rabbit anti-cytochrome-c, mouse anti-8-oxoguanine, AlexaFluor 647-conjugated rabbit anti-histone H2AX [phospho S139], rabbit anti-p-JNK [phospho T183/Y185] (Abcam), rabbit anti-p-c-Jun [phospho S63] (Cell signaling), and rabbit anti-p-ATM (Sigma-Aldrich). The fluorescent-labeled secondary antibodies were AlexaFluor 647-conjugated goat anti-rabbit IgG (Cell Signaling), AlexaFluor 594-conjugated goat anti-mouse IgG (Thermo Scientific), and AlexaFluor 594-conjugated goat anti-mouse IgM (Thermo Scientific). For nuclear counterstaining, we used 4’,6-diamidino-2-phenylindole (DAPI, Life Technologies). Specimens were mounted with Prolong Gold Anti-fade reagent (Life Technologies). Fluorescence-labeled specimens were observed with a Zeiss 780 laser scanning confocal microscope (Carl Zeiss Microscopy GmbH. Jena, Germany).

2.7. Real-time quantitative PCR (qPCR) analysis

Total RNA was extracted from maturation stage rat mandibular incisor enamel organs using Direct-zol RNA MiniPrep (Zymo Research Corp., Irvine, CA). Total RNA was reverse-transcribed into cDNA using a Transcriptor First Strand cDNA Synthesis Kit (Roche Diagnostics, Minneapolis, MN). The cDNA was subjected to qPCR amplification on a LightCycler 480 Real-Time PCR System (Roche Diagnostics). The relative expression of target genes was determined by the $2^{-\Delta\Delta CT}$ method [39]. cDNA from six different rat incisors in each treatment group was assayed in duplicate. The internal reference control gene was *B2m* because of its consistent expression level regardless of fluoride treatment. Primers (Invitrogen) and their sequences were *Ogg1*, forward: 5'-TTGGACCTCGACTCGTTCAG-3', reverse: 5'-GCACTGGCACATACATAGCG-3'; *B2m*, forward: 5'-CGTCGTGCTTGCCATTCAGAA-3', reverse: 5'-GAAGTTGGGCTTCCCATTCTCC-3'.

2.8. Statistical analysis

Western blot and ATP quantification results were analyzed by one-way analysis of variance with Fisher's protected least significant difference post hoc test. Quantification of ROS generation, UCP2, and γH2AX (Western blots) and *Ogg1* (qPCR) were assessed by simple regression analyses. Values of $P < 0.05$ were considered statistically significant.

3. Results

3.1. Fluoride-induced reactive oxygen species generation and inhibition

LS8 cells were treated with 0–10 mM NaF for 3 h and ROS production was measured by the cell-permeant oxidative stress indicator (CM)-H_2DCFDA. Intracellular ROS was significantly induced ($P < 0.001$) by fluoride treatment in a dose-dependent manner (Fig. 1A). In contrast, treatment of LS8 cells with 5 or 10 mM NaCl did not significantly induce ROS levels (Fig. 1S). To identify upstream mediators of ROS induction, we asked if NADPH oxidases (NOX), which catalyze the reduction of molecular oxygen to form the superoxide radical anion ($\bullet O_2^-$) and hydrogen peroxide (H_2O_2), were involved in the fluoride-mediated increase in ROS levels. For these experiments LS8 cells were pretreated for 1 h with 0–500 μM of the NOX inhibitor GTK137831 followed by 3 h treatment with 5 mM NaF. NOX inhibition significantly decreased ROS levels generated by fluoride treatment (Fig. 1B), indicating that NOX is at least partially responsible for fluoride-mediated ROS induction.

3.2. Fluoride induces cytochrome-c release and UCP2 expression and reduces ATP levels

Since ROS causes mitochondrial damage, we analyzed the effect of fluoride on mitochondrial function in LS8 cells. Fluoride treatment (5 mM) for 6 h increased cytochrome-c release into the cytosol as confirmed by the decreasing amount of cytochrome-c within mitochondria (Fig. 2A). UCP2 is an antioxidant located in the inner mitochondrial membrane. ROS increases UCP2, which negatively regulates mitochondrial membrane potential and ATP synthesis during oxidative stress [20]. Recently, we reported that fluoride increases UCP2 expression in rat enamel organ [17]. Here, we confirm the

effects of fluoride on UCP2 expression and ATP synthesis in vitro. LS8 cells were treated with NaF for 6 h at the indicated fluoride concentrations and UCP2 expression was quantified by western blots. Fluoride treatment significantly increased UCP2 expression (Fig. 2B) and decreased intracellular ATP levels (Fig. 2C). These results suggest that the fluoride-mediated increase in intracellular ROS induces oxidative stress, which impairs mitochondrial function as observed by cytochrome-c release, UCP2 induction, and reduced ATP synthesis.

3.3. Fluoride induces SIRT1/autophagy through the ROS-MAPKKK-JNK/c-Jun pathway

Recently we reported that fluoride activates SIRT1/autophagy as an adaptive response [24]. Previously we demonstrated that fluoride elicits JNK signaling to phosphorylate JNK and c-Jun [13]. Since JNK signaling can phosphorylate SIRT1 to promote SIRT1 deacetylase activity [35], we asked if JNK signaling is involved in fluoride-induced SIRT1 activation. LS8 cells were treated with 10 or 30 μM of the JNK inhibitor SP600125 for 1 h prior to 2 h 5 mM fluoride treatment. Fluoride-induced JNK and c-Jun phosphorylation were significantly decreased by JNK inhibition (Fig. 3A). JNK inhibition also attenuated fluoride-induced SIRT1 phosphorylation after 6 h fluoride treatment (Fig. 3B). These results indicate that fluoride activates SIRT1 in a JNK-dependent manner.

To determine if the JNK inhibitor had any effect on fluoride-induced ROS production, LS8 cells were pretreated for 1 h with 10 or 30 μM SP600125 followed by 3 h treatment with or without 5 mM NaF. JNK inhibition did not significantly affect fluoride-induced ROS levels (Fig. 2S), indicating that JNK activation occurs after ROS induction. Similar conditions were used to demonstrate that after 6 h of fluoride treatment, JNK inhibition had no effect on ROS-mediated mitochondria cytochrome-c release in LS8 cells (Fig. 3S). However, when we treated cells with 10 or 100 nM of the TAK1 (MAP3K7) inhibitor oxozeaenol, we observed significant decreases in fluoride-mediated activation of JNK and c-Jun (Fig. 4), suggesting that the MAPKKK pathway plays a role in activating JNK and c-Jun. Therefore, fluoride promotes ROS production through NOX induction, causing mitochondria to increase UCP2 expression, which leads to reduced ATP syntheses and release of cytochrome-c. ROS also activates the MAPKKK pathway, which activates JNK, which, in turn, activates the SIRT1/autophagy adaptive response.

3.4. The antioxidant N-acetylcysteine (NAC) attenuates ROS-mediated JNK activation

Next, we asked if NAC attenuates ROS-mediated JNK activation and the downstream fluoride-induced SIRT1/autophagy adaptive response. LS8 cells were treated with increasing concentrations NAC for 1 h prior to 10 mM fluoride treatment for 3 h. NAC significantly decreased fluoride-induced ROS production in a dose-dependent manner (Fig. 5A). NAC treatment for 2 h also attenuated fluoride-induced phosphorylation of JNK and c-Jun (Fig. 5B). After 6 h treatment, this reduction in JNK activation resulted in decreased SIRT1 phosphorylation (Fig. 5C) and diminished induction of autophagy, as measured by LC3II formation (Fig. 5D). These results confirm that fluoride activates SIRT1/autophagy via ROS-mediated JNK signaling.

3.5. Fluoride treatment induces a DNA damage response in LS8 cells and NAC exacerbates this response

In mammalian cells, histone H2AX phosphorylation (γH2AX) is the hallmark of a DNA damage response. γH2AX accumulates at DNA damage sites to recruit the DNA repair complex. Since ROS exposure can result in DNA damage, we asked if DNA damage occurs as a result of fluoride treatment in LS8 cells. Fluoride (0–5 mM) treatment for 6 h did induce H2AX phosphorylation (Fig. 6). This result confirms previous results obtained by different methodologies showing that fluoride is capable of inducing apoptosis-mediated DNA fragmentation in LS8 cells [15].

Next we asked if NAC, which attenuates fluoride-induced SIRT1/autophagy (Fig. 5C, D), has any effect on fluoride-mediated DNA damage and apoptosis. LS8 cells were treated with or without 5 or 10 mM NAC for 1 h prior to 5 mM fluoride treatment. Western blots demonstrated that NAC treatment increased the levels both of γH2AX after 6 h and of cleaved caspase-3 after 6 and 18 h (Fig. 7). These unexpected results have been observed by others [40–42]. It is possible that the role of ROS in activating SIRT1/autophagy as an adaptive response is necessary to protect cells from fluoride-induced apoptosis.

3.6. Fluoride-induced DNA and mitochondrial damage in vivo

To determine if fluoride causes DNA and/or mitochondria damage in vivo, six-week-old rats or mice were provided 0, 50, 100, or 125 ppm fluoride as NaF ad libitum in drinking water. As a reference, 19 ppm = 1 mM fluoride. After 6 weeks of fluoride treatment, maxillary incisors were subjected to immunohistochemical analysis. Shown (Fig. 8) are secretory (SEC)- and maturation (MAT)-stage rat or mouse ameloblasts stained with antisera specific for cytochrome-c, 8-oxoguanine, p-JNK, p-ATM, or γH2AX. In the fluoride treatment groups, maturation-stage ameloblasts stained strongly for cytochrome-c (Fig. 8A) and p-JNK (Fig. 8C), and the DNA damage markers 8-oxoguanine, p-ATM, and γH2AX also stained positively in the maturation-stage fluoride treatment groups (Fig. 8B, D, E). Interestingly, the fluoride-treated secretory stage ameloblasts also had strong positive staining for 8-oxoguanine. These data suggest that fluoride causes DNA and mitochondrial damage that may contribute to the pathology of dental fluorosis.

4. Discussion

Previously we reported that fluoride induces cell stress such as ER stress [15,16] and oxidative stress [17] that may play a role in dental fluorosis. Recently we demonstrated that fluoride activates SIRT1 and autophagy as adaptive responses to protect cells from fluoride-induced cytotoxicity [24]. However, the mechanisms underlying fluoride and oxidative stress in dental fluorosis remain obscure. Here we demonstrate that fluoride promotes ROS production through NOX induction, which causes mitochondria to increase UCP2 expression, which leads to reduced ATP syntheses and promotes cytochrome-c release. ROS also causes DNA damage and can activate the MAPKKK pathway. This activates JNK, which, in turn, activates the SIRT1/autophagy adaptive response.

Fluoride is an essential trace element required for human and animal health. Since low-dose fluoride is an effective prophylactic for dental caries, it is used for water fluoridation. Fluoride in drinking water at 0.7 ppm reduces dental caries, but fluoride concentrations significantly above this level can cause enamel and skeletal fluorosis, renal toxicity, diarrhea, epithelial lung cell toxicity, and heart rate disorders [43–45]. Numerous studies have revealed a close association between chronic fluoride toxicity and increased ROS levels with resulting oxidative stress in such organs as the liver, kidney, brain, and heart [46,47]. However, it is not clear how fluoride-induced oxidative stress is involved in the pathology of dental fluorosis.

Previously we reported that the oxidative stress response gene *Ucp2* was up-regulated at the mRNA and protein level by fluoride treatment in rat maturation stage enamel organs [17]. UCP2 is located in the mitochondria and it responds to high ROS levels by down-regulating mitochondrial ROS production. It does this by attenuating ATP production necessary for such activities as glucose metabolism [20,48]. In the present study, we show that fluoride induced ROS production through NOX activation (Fig. 1). Fluoride also caused mitochondrial damage, as observed by cytochorome-c release, and caused induction of UCP2 expression in order to reduce ATP synthesis necessary to diminish overall ROS levels (Fig. 2). Rats treated with 100 or 125 ppm fluoride in their drinking water had ameloblasts that also released cytochrome-c into their cytoplasm (Fig. 8A). These results suggest that fluoride induces mitochondrial dysfunction through the ROS-UCP2 pathway and that this may contribute to an inability of ameloblasts to completely remove enamel matrix proteins during the maturation stage of enamel formation. This helps explain why fluorosed enamel is softer than normal because of a higher than normal protein content [49].

As described above, excess ROS can have detrimental consequences, including mitochondrial damage and DNA damage. However, under certain conditions, ROS can serve as redox messengers in the regulation of cellular metabolism, promote antioxidant defense, and play a role in the posttranslational modification of proteins. ROS-mediated JNK signaling was reported to activate SIRT1 [35]. The ROS-JNK pathway also activates autophagy to promote cell survival during ER stress [50]. In this study, we evaluated the effect of NAC (antioxidant) and SP600125 (JNK inhibitor) on the fluoride-induced activation of SIRT1/autophagy. Treatment with SP600125 decreased fluoride-induced p-SIRT1 formation in LS8 cells (Fig. 3B). NAC treatment attenuated fluoride-induced formation of p-JNK, p-c-Jun, p-SIRT1, and LC3II (Fig. 5). These results suggest that fluoride activates SIRT1/autophagy through ROS-mediated JNK signaling.

Previous studies revealed that fluoride can cause DNA damage in various tissues such as bone marrow, liver, kidney, and spleen, which may occur through fluoride-induced ROS production [51,52]. However, the genotoxic effects of fluoride in the enamel organ have not been extensively investigated. Moreover, current literature about the genotoxic potential of fluoride in various cells and/or tissues is contradictory. Studies have shown that fluoride does not induce DNA damage [53–55], whereas other studies have observed fluoride-induced DNA damage in rat and human cells [52,56,57]. The possible mechanisms of fluoride-induced DNA damage are that (1) fluoride directly attacks the free amine groups present in DNA or (2) fluoride acts indirectly through free radicals to create DNA adducts at

hydrogen bonds [58]. JNK signaling can induce phosphorylation of histone H2AX (γH2AX), which recruits the DNA repair complex or signals for caspase-mediated DNA fragmentation [23]. We demonstrate that fluoride induces γH2AX formation in LS8 cells (Fig. 6). Induction of DNA damage markers, (p-ATM and γH2AX) and an increase in 8-oxoguanine levels were also observed in fluoride-treated rat or mouse ameloblasts (Fig. 8).

8-Oxoguanine-DNA glycosylase (OGG1) recognizes and excises 8-oxoguanine lesions [59]. The response of OGG1 to oxidative stress does not always result in an increase in its activity [60,61]. The transcriptional expression of *Ogg1* is consistent neither with protein expression levels nor with OGG1 activity [62–65]. We found that fluoride treatment did not significantly change *Ogg1* mRNA levels in rat enamel organ (Fig. 4S). Initially we were surprised by the NAC-mediated increase in γH2AX formation and caspase-3 activation (Fig. 7), because NAC has been shown to protect against drug- and oxidative-stress-induced apoptosis [66–68]. But, with further investigation, we found that NAC has also been shown to induce apoptosis in various cell types via mitochondrial-dependent and ROS-independent means, by ER-stress-response-signaling pathways, and/or by ATP depletion [40–42]. NAC appears to function differently depending on the cell type, and LS8 cells were found to be susceptible to NAC toxicity. Additionally, NAC treatment attenuated the adaptive SIRT1/autophagy response (Fig. 4), which may also promote apoptosis. Moreover, the results in this study are also consistent with our previous study demonstrating that the antioxidant vitamin E did not ameliorate mouse dental fluorosis [17]. These results suggest that fluoride-induced ROS generation may play both a genotoxic role (8-oxoguanine increase) and a protective role as a redox messenger to stimulate an adaptive response involving SIRT1 and autophagy. See Fig. 9 for a summary.

In conclusion, fluoride-induced ROS generation causes oxidative damage to mitochondria and DNA in LS8 cells and/or ameloblasts. But fluoride activates SIRT1/autophagy via ROS-mediated JNK signaling to protect cells from fluoride-induced cytotoxicity. Elimination of ROS by the antioxidant NAC did not mitigate fluoride-induced toxicity but instead increased the DNA damage marker γH2AX and increased the level of cleaved caspase-3 that mediates apoptosis. These results suggest that fluoride-induced ROS production may play a protective role by activating SIRT1/autophagy. Enhancing ROS-mediated JNK signaling, without the associated mitochondria and DNA damage, could offer a novel strategy for treatments to prevent dental fluorosis.

Supplementary Material

Refer to Web version on PubMed Central for supplementary material.

Acknowledgments

We thank Justine Dobeck for histology expertise and Dr. Malcolm L. Snead for generously providing us with LS8 cells. Research reported in this publication was supported by the National Institute of Dental and Craniofacial Research of the National Institutes of Health under Award R01DE018106.

References

1. CDC. Recommendations for using fluoride to prevent and control dental caries in the United States. Centers for Disease Control and Prevention. MMWR. Recommendations and reports: Morbidity and mortality weekly report. Recommendations and reports/Centers for Disease Control. 2001; 50:1–42.
2. Dean HT, Elvove E. Some Epidemiological Aspects of Chronic Endemic Dental Fluorosis. American journal of public health and the nation's health. 1936; 26:567–575.
3. Boivin G, Chavassieux P, Chapuy MC, Baud CA, Meunier PJ. Skeletal fluorosis: histomorphometric analysis of bone changes and bone fluoride content in 29 patients. Bone. 1989; 10:89–99. [PubMed: 2765315]
4. Zager RA, Iwata M. Inorganic fluoride. Divergent effects on human proximal tubular cell viability. The American journal of pathology. 1997; 150:735–745. [PubMed: 9033286]
5. Thrane EV, Refsnes M, Thoresen GH, Lag M, Schwarze PE. Fluoride-induced apoptosis in epithelial lung cells involves activation of MAP kinases p38 and possibly JNK. Toxicological sciences: an official journal of the Society of Toxicology. 2001; 61:83–91. [PubMed: 11294978]
6. Ghosh D, Das Sarkar S, Maiti R, Jana D, Das UB. Testicular toxicity in sodium fluoride treated rats: association with oxidative stress. Reproductive toxicology. 2002; 16:385–390. [PubMed: 12220599]
7. Sun Z, Niu R, Wang B, Jiao Z, Wang J, Zhang J, Wang S, Wang J. Fluoride-induced apoptosis and gene expression profiling in mice sperm in vivo. Archives of toxicology. 2011; 85:1441–1452. [PubMed: 21340527]
8. DenBesten PK. Biological mechanisms of dental fluorosis relevant to the use of fluoride supplements. Community dentistry and oral epidemiology. 1999; 27:41–47. [PubMed: 10086925]
9. Kotecha PV, Patel SV, Bhalani KD, Shah D, Shah VS, Mehta KG. Prevalence of dental fluorosis & dental caries in association with high levels of drinking water fluoride content in a district of Gujarat, India. The Indian journal of medical research. 2012; 135:873–877. [PubMed: 22825606]
10. Beltran-Aguilar ED, Barker L, Dye BA. Prevalence and severity of dental fluorosis in the United States, 1999–2004. NCHS data brief. 2010:1–8. [PubMed: 21211168]
11. Hu JC, Chun YH, Al Hazzazzi T, Simmer JP. Enamel formation and amelogenesis imperfecta. Cells, tissues, organs. 2007; 186:78–85. [PubMed: 17627121]
12. Smith CE, Issid M, Margolis HC, Moreno EC. Developmental changes in the pH of enamel fluid and its effects on matrix-resident proteinases. Advances in dental research. 1996; 10:159–169. [PubMed: 9206332]
13. Sharma R, Tsuchiya M, Skobe Z, Tannous BA, Bartlett JD. The acid test of fluoride: how pH modulates toxicity. PloS one. 2010; 5:e10895. [PubMed: 20531944]
14. Ito M, Nakagawa H, Okada T, Miyazaki S, Matsuo S. ER-stress caused by accumulated intracistanal granules activates autophagy through a different signal pathway from unfolded protein response in exocrine pancreas cells of rats exposed to fluoride. Archives of toxicology. 2009; 83:151–159. [PubMed: 18696052]
15. Kubota K, Lee DH, Tsuchiya M, Young CS, Everett ET, Martinez-Mier EA, Snead ML, Nguyen L, Urano F, Bartlett JD. Fluoride induces endoplasmic reticulum stress in ameloblasts responsible for dental enamel formation. The Journal of biological chemistry. 2005; 280:23194–23202. [PubMed: 15849362]
16. Sharma R, Tsuchiya M, Bartlett JD. Fluoride induces endoplasmic reticulum stress and inhibits protein synthesis and secretion. Environmental health perspectives. 2008; 116:1142–1146. [PubMed: 18795154]
17. Suzuki M, Sierant ML, Antone JV, Everett ET, Whitford GM, Bartlett JD. Uncoupling protein-2 is an antioxidant that is up-regulated in the enamel organ of fluoride-treated rats. Connective tissue research. 2014; 55(Suppl 1):25–28. [PubMed: 25158175]
18. Izquierdo-Vega JA, Sanchez-Gutierrez M, Del Razo LM. Decreased in vitro fertility in male rats exposed to fluoride-induced oxidative stress damage and mitochondrial transmembrane potential loss. Toxicology and applied pharmacology. 2008; 230:352–357. [PubMed: 18455746]

19. Garcia-Montalvo EA, Reyes-Perez H, Del Razo LM. Fluoride exposure impairs glucose tolerance via decreased insulin expression and oxidative stress. Toxicology. 2009; 263:75–83. [PubMed: 19540901]
20. Mailloux RJ, Harper ME. Uncoupling proteins and the control of mitochondrial reactive oxygen species production. Free radical biology & medicine. 2011; 51:1106–1115. [PubMed: 21762777]
21. Celeste A, Petersen S, Romanienko PJ, Fernandez-Capetillo O, Chen HT, Sedelnikova OA, Reina-San-Martin B, Coppola V, Meffre E, Difllippantonio MJ, Redon C, Pilch DR, Olaru A, Eckhaus M, Camerini-Otero RD, Tessarollo L, Livak F, Manova K, Bonner WM, Nussenzweig MC, Nussenzweig A. Genomic instability in mice lacking histone H2AX. Science. 2002; 296:922–927. [PubMed: 11934988]
22. Celeste A, Fernandez-Capetillo O, Kruhlak MJ, Pilch DR, Staudt DW, Lee A, Bonner RF, Bonner WM, Nussenzweig A. Histone H2AX phosphorylation is dispensable for the initial recognition of DNA breaks. Nature cell biology. 2003; 5:675–679.
23. Sluss HK, Davis RJ. H2AX is a target of the JNK signaling pathway that is required for apoptotic DNA fragmentation. Molecular cell. 2006; 23:152–153. [PubMed: 16857581]
24. Suzuki M, Bartlett JD. Sirtuin1 and autophagy protect cells from fluoride-induced cell stress. Biochimica et biophysica acta. 2014; 1842:245–255. [PubMed: 24296261]
25. Landry J, Sutton A, Tafrov ST, Heller RC, Stebbins J, Pillus L, Sternglanz R. The silencing protein SIR2 and its homologs are NAD-dependent protein deacetylases. Proceedings of the National Academy of Sciences of the United States of America. 2000; 97:5807–5811. [PubMed: 10811920]
26. Imai S, Armstrong CM, Kaeberlein M, Guarente L. Transcriptional silencing and longevity protein Sir2 is an NAD-dependent histone deacetylase. Nature. 2000; 403:795–800. [PubMed: 10693811]
27. Smith JS, Brachmann CB, Celic I, Kenna MA, Muhammad S, Starai VJ, Avalos JL, Escalante-Semerena JC, Grubmeyer C, Wolberger C, Boeke JD. A phylogenetically conserved NAD+-dependent protein deacetylase activity in the Sir2 protein family. Proceedings of the National Academy of Sciences of the United States of America. 2000; 97:6658–6663. [PubMed: 10841563]
28. Nemoto S, Fergusson MM, Finkel T. Nutrient availability regulates SIRT1 through a forkhead-dependent pathway. Science. 2004; 306:2105–2108. [PubMed: 15604409]
29. Blander G, Guarente L. The Sir2 family of protein deacetylases. Annual review of biochemistry. 2004; 73:417–435.
30. Salminen A, Kaarniranta K, Kauppinen A. Crosstalk between Oxidative Stress and SIRT1: Impact on the Aging Process. International journal of molecular sciences. 2013; 14:3834–3859. [PubMed: 23434668]
31. Nogueiras R, Habegger KM, Chaudhary N, Finan B, Banks AS, Dietrich MO, Horvath TL, Sinclair DA, Pfluger PT, Tschop MH. Sirtuin 1 and sirtuin 3: physiological modulators of metabolism. Physiological reviews. 2012; 92:1479–1514. [PubMed: 22811431]
32. Hayashida S, Arimoto A, Kuramoto Y, Kozako T, Honda S, Shimeno H, Soeda S. Fasting promotes the expression of SIRT1, an NAD+ -dependent protein deacetylase, via activation of PPARalpha in mice. Molecular and cellular biochemistry. 2010; 339:285–292. [PubMed: 20148352]
33. Han L, Zhou R, Niu J, McNutt MA, Wang P, Tong T. SIRT1 is regulated by a PPAR{gamma}-SIRT1 negative feedback loop associated with senescence. Nucleic acids research. 2010; 38:7458–7471. [PubMed: 20660480]
34. Noriega LG, Feige JN, Canto C, Yamamoto H, Yu J, Herman MA, Mataki C, Kahn BB, Auwerx J. CREB and ChREBP oppositely regulate SIRT1 expression in response to energy availability. EMBO reports. 2011; 12:1069–1076. [PubMed: 21836635]
35. Nasrin N, Kaushik VK, Fortier E, Wall D, Pearson KJ, de Cabo R, Bordone L. JNK1 phosphorylates SIRT1 and promotes its enzymatic activity. PloS one. 2009; 4:e8414. [PubMed: 20027304]
36. Houtkooper RH, Pirinen E, Auwerx J. Sirtuins as regulators of metabolism and healthspan. Nature reviews. Molecular cell biology. 2012; 13:225–238.
37. Canto C, Gerhart-Hines Z, Feige JN, Lagouge M, Noriega L, Milne JC, Elliott PJ, Puigserver P, Auwerx J. AMPK regulates energy expenditure by modulating NAD+ metabolism and SIRT1 activity. Nature. 2009; 458:1056–1060. [PubMed: 19262508]

38. Chen LS, Couwenhoven RI, Hsu D, Luo W, Snead ML. Maintenance of amelogenin gene expression by transformed epithelial cells of mouse enamel organ. Archives of oral biology. 1992; 37:771–778. [PubMed: 1444889]
39. Pfaf MW. A new mathematical model for relative quantification in real-time RT-PCR. Nucleic acids research. 2001; 29:e45. [PubMed: 11328886]
40. Yang J, Su Y, Richmond A. Antioxidants tiron and N-acetyl-l-cysteine differentially mediate apoptosis in melanoma cells via a reactive oxygen species-independent NF-kappaB pathway. Free radical biology & medicine. 2007; 42:1369–1380. [PubMed: 17395010]
41. Guan D, Xu Y, Yang M, Wang H, Wang X, Shen Z. N-acetyl cysteine and penicillamine induce apoptosis via the ER stress response-signaling pathway. Molecular carcinogenesis. 2010; 49:68–74. [PubMed: 19722195]
42. Ma Z, Wei Q, Dong G, Huo Y, Dong Z. DNA damage response in renal ischemia-reperfusion and ATP-depletion injury of renal tubular cells. Biochimica et biophysica acta. 2014; 1842:1088–1096. [PubMed: 24726884]
43. Fordyce FM, Vrana K, Zhovinsky E, Povoroznuk V, Toth G, Hope BC, Iljinsky U, Baker J. A health risk assessment for fluoride in Central Europe. Environmental geochemistry and health. 2007; 29:83–102. [PubMed: 17256094]
44. Everett ET. Fluoride's effects on the formation of teeth and bones, and the influence of genetics. Journal of dental research. 2011; 90:552–560. [PubMed: 20929720]
45. Sauerheber R. Physiologic conditions affect toxicity of ingested industrial fluoride. Journal of environmental and public health. 2013; 2013:439490. [PubMed: 23840230]
46. Chouhan S, Flora SJ. Effects of fluoride on the tissue oxidative stress and apoptosis in rats: biochemical assays supported by IR spectroscopy data. Toxicology. 2008; 254:61–67. [PubMed: 18845224]
47. Flora SJ, Mittal M, Pachauri V, Dwivedi N. A possible mechanism for combined arsenic and fluoride induced cellular and DNA damage in mice. Metallomics: integrated biometal science. 2012; 4:78–90. [PubMed: 21986897]
48. Krauss S, Zhang CY, Scorrano L, Dalgaard LT, St-Pierre J, Grey ST, Lowell BB. Superoxide-mediated activation of uncoupling protein 2 causes pancreatic beta cell dysfunction. The Journal of clinical investigation. 2003; 112:1831–1842. [PubMed: 14679178]
49. Wright JT, Chen SC, Hall KI, Yamauchi M, Bawden JW. Protein characterization of fluorosed human enamel. Journal of dental research. 1996; 75:1936–1941. [PubMed: 9033447]
50. Ogata M, Hino S, Saito A, Morikawa K, Kondo S, Kanemoto S, Murakami T, Taniguchi M, Tanii I, Yoshinaga K, Shiosaka S, Hammarback JA, Urano F, Imaizumi K. Autophagy is activated for cell survival after endoplasmic reticulum stress. Molecular and cellular biology. 2006; 26:9220–9231. [PubMed: 17030611]
51. He LF, Chen JG. DNA damage, apoptosis and cell cycle changes induced by fluoride in rat oral mucosal cells and hepatocytes. World journal of gastroenterology: WJG. 2006; 12:1144–1148.
52. Sinha MJS, Ghosh M, Mukherjee A. Evaluation of multi-endpoint assay to detect genotoxicity and oxidative stress in mice exposed to sodium fluoride. Mutation research. 2013; 751:59–65. [PubMed: 23201538]
53. Ribeiro DA, Marques ME, de Assis GF, Anzai A, Poleti ML, Salvadori DM. No relationship between subchronic fluoride intake and DNA damage in Wistar rats. Caries research. 2004; 38:576–579. [PubMed: 15528915]
54. Slamenova D, Gabelova A, Ruppova K. Cytotoxicity and genotoxicity testing of sodium fluoride on Chinese hamster V79 cells and human EUE cells. Mutation research. 1992; 279:109–115. [PubMed: 1375335]
55. Shanthakumari D, Srinivasalu S, Subramanian S. Effect of fluoride intoxication on lipidperoxidation and antioxidant status in experimental rats. Toxicology. 2004; 204:219–228. [PubMed: 15388248]
56. Rao SM, Sherlin HJ, Anuja N, Pratibha R, Priya P, Chandrasekar T. Morphometry of buccal mucosal cells in fluorosis–a new paradigm. Human & experimental toxicology. 2011; 30:1761–1768. [PubMed: 21406483]

57. Pal S, Sarkar C. Protective effect of resveratrol on fluoride induced alteration in protein and nucleic acid metabolism, DNA damage and biogenic amines in rat brain. Environmental toxicology and pharmacology. 2014; 38:684–699. [PubMed: 25233527]

58. Flora SJ, Mittal M, Mishra D. Co-exposure to arsenic and fluoride on oxidative stress, glutathione linked enzymes, biogenic amines and DNA damage in mouse brain. Journal of the neurological sciences. 2009; 285:198–205. [PubMed: 19635623]

59. Bruner SD, Norman DP, Verdine GL. Structural basis for recognition and repair of the endogenous mutagen 8-oxoguanine in DNA. Nature. 2000; 403:859–866. [PubMed: 10706276]

60. Bravard A, Vacher M, Gouget B, Coutant A, de Boisferon FH, Marsin S, Chevillard S, Radicella JP. Redox regulation of human OGG1 activity in response to cellular oxidative stress. Molecular and cellular biology. 2006; 26:7430–7436. [PubMed: 16923968]

61. Cortina MS, Gordon WC, Lukiw WJ, Bazan NG. Oxidative stress-induced retinal damage up-regulates DNA polymerase gamma and 8-oxoguanine-DNA-glycosylase in photoreceptor synaptic mitochondria. Experimental eye research. 2005; 81:742–750. [PubMed: 15979612]

62. Saitoh T, Shinmura K, Yamaguchi S, Tani M, Seki S, Murakami H, Nojima Y, Yokota J. Enhancement of OGG1 protein AP lyase activity by increase of APEX protein. Mutation research. 2001; 486:31–40. [PubMed: 11356334]

63. Jin L, Yang H, Fu J, Xue X, Yao L, Qiao L. Association between oxidative DNA damage and the expression of 8-oxoguanine DNA glycosylase 1 in lung epithelial cells of neonatal rats exposed to hyperoxia. Molecular medicine reports. 2015; 11:4079–4086. [PubMed: 25672835]

64. Kershaw RM, Hodges NJ. Repair of oxidative DNA damage is delayed in the Ser326Cys polymorphic variant of the base excision repair protein OGG1. Mutagenesis. 2012; 27:501–510. [PubMed: 22451681]

65. Kaur MP, Guggenheim EJ, Pulisciano C, Akbar S, Kershaw RM, Hodges NJ. Cellular accumulation of Cys326-OGG1 protein complexes under conditions of oxidative stress. Biochemical and biophysical research communications. 2014; 447:12–18. [PubMed: 24680828]

66. Luczak MW, Zhitkovich A. Role of direct reactivity with metals in chemo-protection by N-acetylcysteine against chromium(VI), cadmium(II), and cobalt (II). Free radical biology & medicine. 2013; 65:262–269. [PubMed: 23792775]

67. Jin HM, Zhou DC, Gu HF, Qiao QY, Fu SK, Liu XL, Pan Y. Antioxidant N-acetylcysteine protects pancreatic beta-cells against aldosterone-induced oxidative stress and apoptosis in female db/db mice and insulin-producing MIN6 cells. Endocrinology. 2013; 154:4068–4077. [PubMed: 24008345]

68. Ji YL, Wang H, Zhang C, Zhang Y, Zhao M, Chen YH, Xu DX. N-acetylcysteine protects against cadmium-induced germ cell apoptosis by inhibiting endoplasmic reticulum stress in testes. Asian journal of andrology. 2013; 15:290–296. [PubMed: 23353715]

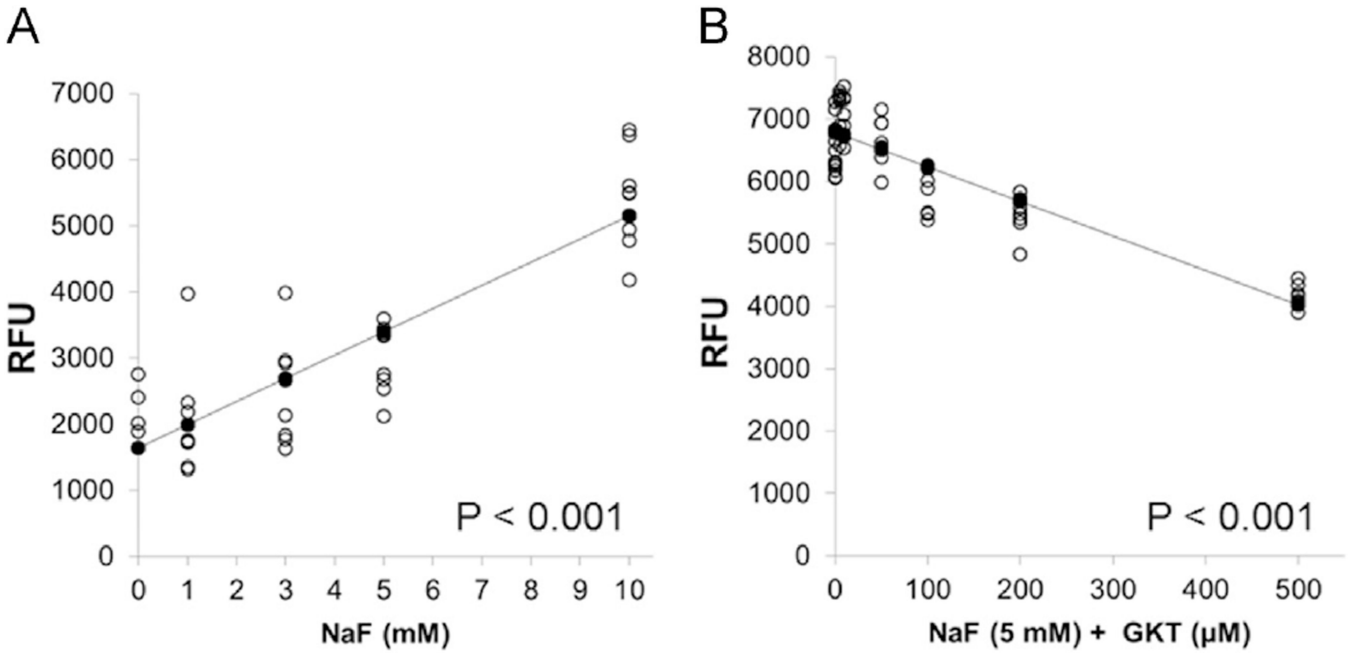

Fig. 1.

Fluoride treatment induces ROS production. (A) LS8 cells were treated with 0–10 mM fluoride for 3 h and intracellular ROS was detected with H_2DCFDA. Upon oxidation by ROS, the nonfluorescent H_2DCFDA is converted to the highly fluorescent 2',7'-dichlorofluorescein (DCF). Regression analysis revealed a highly significant positive correlation between fluoride dose and ROS generation ($P < 0.001$). (B) LS8 cells were treated with 0–500 μM of NOX1/4 inhibitor (GKT137831) for 1 h followed by 5 mM fluoride for 3 h. Intracellular ROS was detected by H_2DCFDA. Regression analysis revealed a highly significant negative correlation between NOX1/4 inhibitor dose and ROS generation after fluoride treatment ($P < 0.001$).

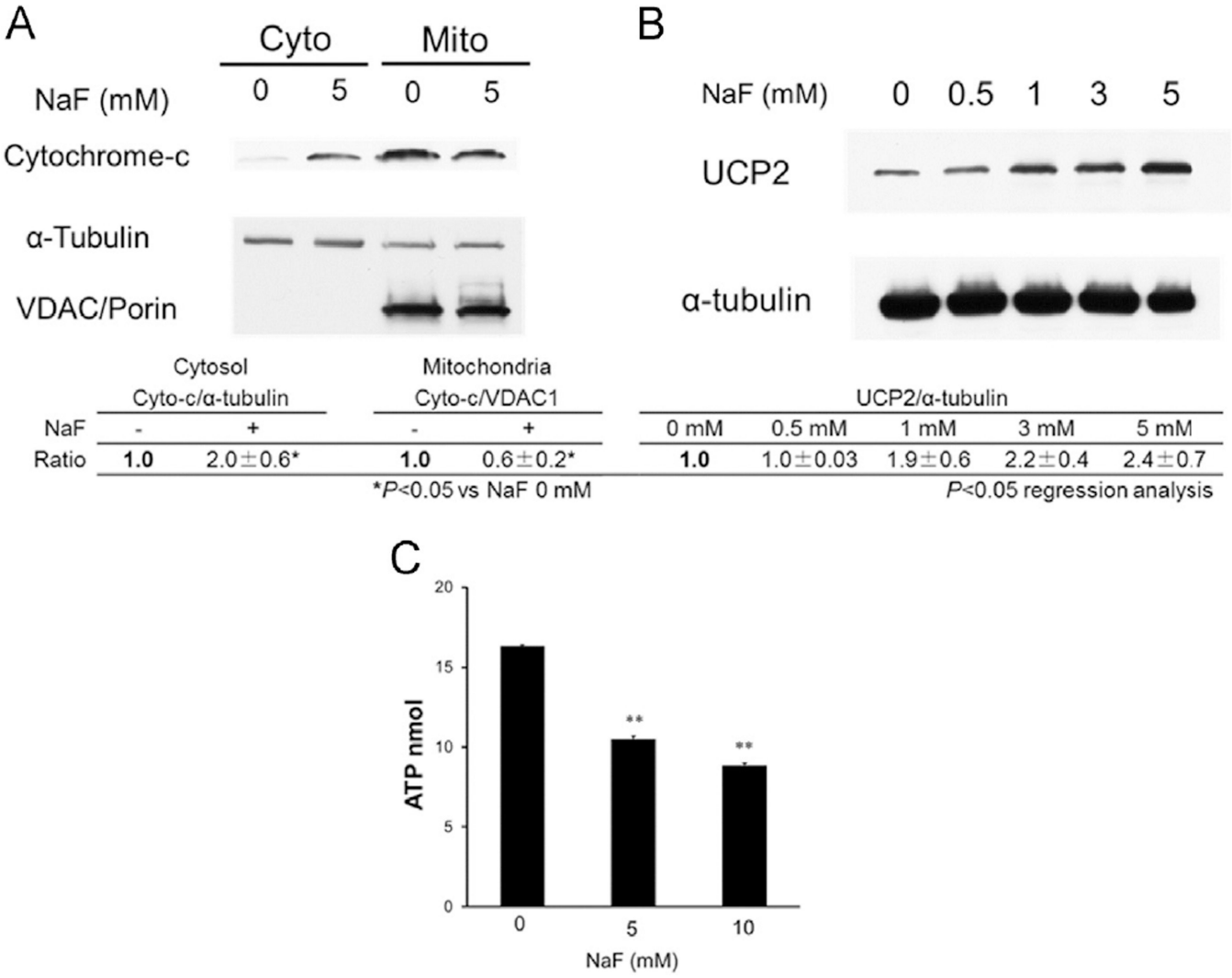

Fig. 2.

Fluoride negatively affects mitochondria function. (A) LS8 cells were treated with 0 or 5 mM fluoride for 6 h and cytochrome-c (12 kDa) levels in the cytosol fraction (Cyto) or in the mitochondrial fraction (Mito) were quantified by western blot analysis. Fluoride treatment released cytochrome c from the mitochondria into the cytosol. α-Tubulin (52 kDa) and VDAC1/porin (31 kDa) were the loading control proteins. The table shows the ratio of cytochrome c/α-tubulin (for cytosol) or cytochrome c/VDAC1 (for mitochondria). *$P < 0.05$ vs. 0 mM of fluoride. (B) LS8 cells were treated with 0–5 mM fluoride for 6 h and total protein was extracted. UCP2 (dimer: 70 kDa) was detected by western blots and levels increased with increasing concentrations of fluoride. α-Tubulin served as a loading control protein. The table shows the UCP2/α-tubulin ratio. Regression analysis revealed a significant positive correlation between fluoride dose and UCP2 expression ($P < 0.05$). (C) LS8 cells were treated with 0, 5, or 10 mM fluoride for 6 h and intracellular ATP was measured by a method that utilizes glycerol phosphorylation, which is quantified by colorimetery (570 nm). ATP levels decreased with increasing fluoride concentrations. Data are expressed as mean ± SD. **$p < 0.01$ vs. 0 mM of fluoride.

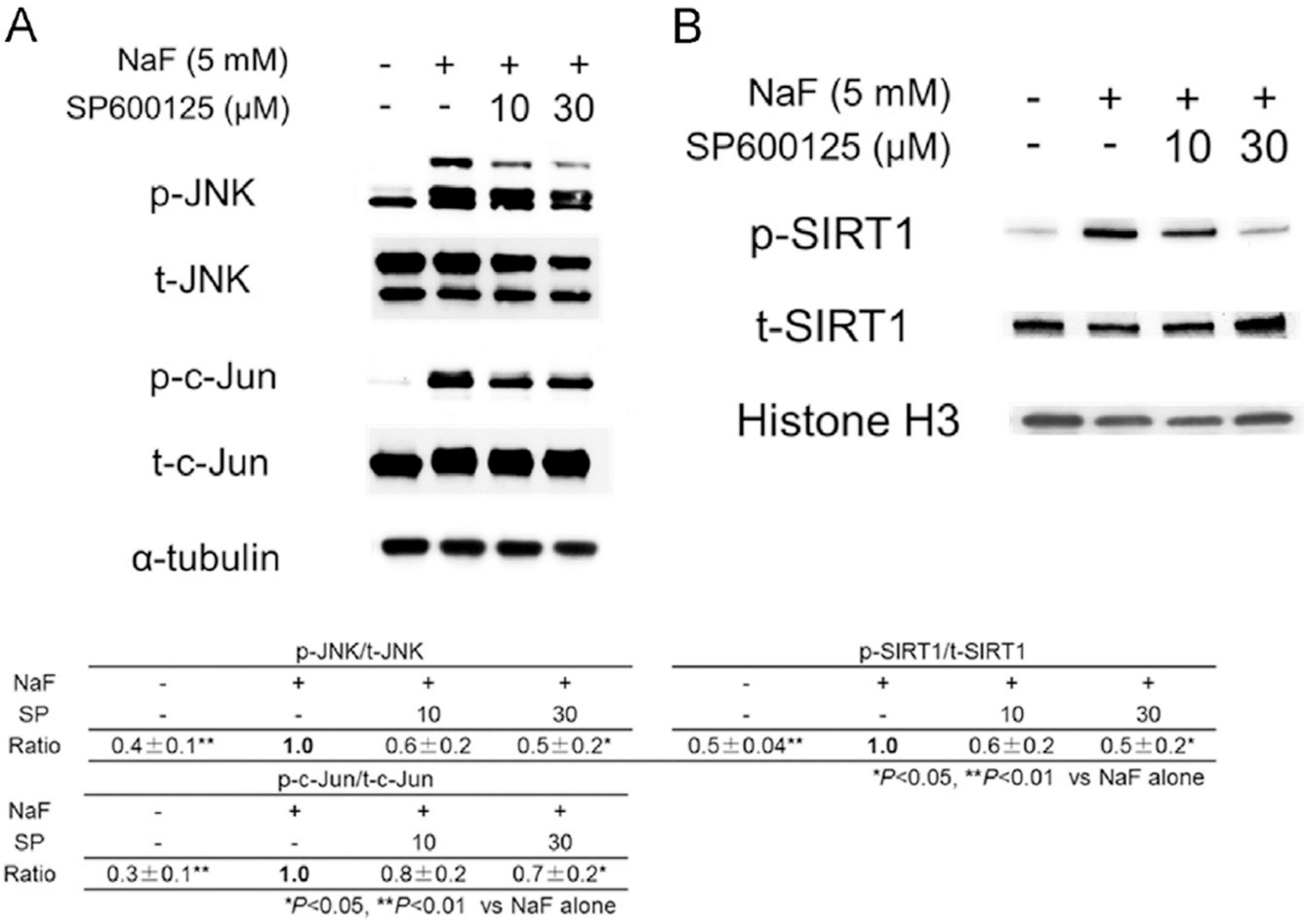

p-JNK/t-JNK				
NaF	-	+	+	+
SP	-	-	10	30
Ratio	0.4±0.1**	**1.0**	0.6±0.2	0.5±0.2*

p-SIRT1/t-SIRT1			
-	+	+	+
-	-	10	30
0.5±0.04**	**1.0**	0.6±0.2	0.5±0.2*

*P<0.05, **P<0.01 vs NaF alone

p-c-Jun/t-c-Jun			
NaF	-	+	+	+
SP	-	-	10	30
Ratio	0.3±0.1**	**1.0**	0.8±0.2	0.7±0.2*

*P<0.05, **P<0.01 vs NaF alone

Fig. 3.

Fluoride induces SIRT1 phosphorylation (p-SIRT) via JNK signaling. LS8 cells were treated with JNK inhibitor SP600125 (10 or 30 μM) for 1 h prior to 5 mM fluoride treatment for 2 h or 6 h. (A) Total protein was extracted at 2 h and phospho-(p)-JNK (46, 54 kDa), total-(t)-JNK (46, 54 kDa), phospho-(p)-c-Jun (48 kDa), and total-(t)-c-Jun (48 kDa) were quantified by western blot analysis. Note that SP600125 treatment reduced the overall levels of p-JNK and p-c-Jun after exposure to fluoride. (B) Nuclear protein was extracted at 6 h and p-SIRT1 (82 kDa) and total-(t)-SIRT1 (120 kDa) were quantified by western blots. SP600125 treatment decreased p-SIRT1 levels after exposure to fluoride. Histone H3 (17 kDa) was the loading control protein. The tables show the ratios p-JNK/t-JNK, p-c-Jun/t-c-Jun, and p-SIRT1/t-SIRT1. *P < 0.05, **p < 0.01 vs. fluoride treatment alone.

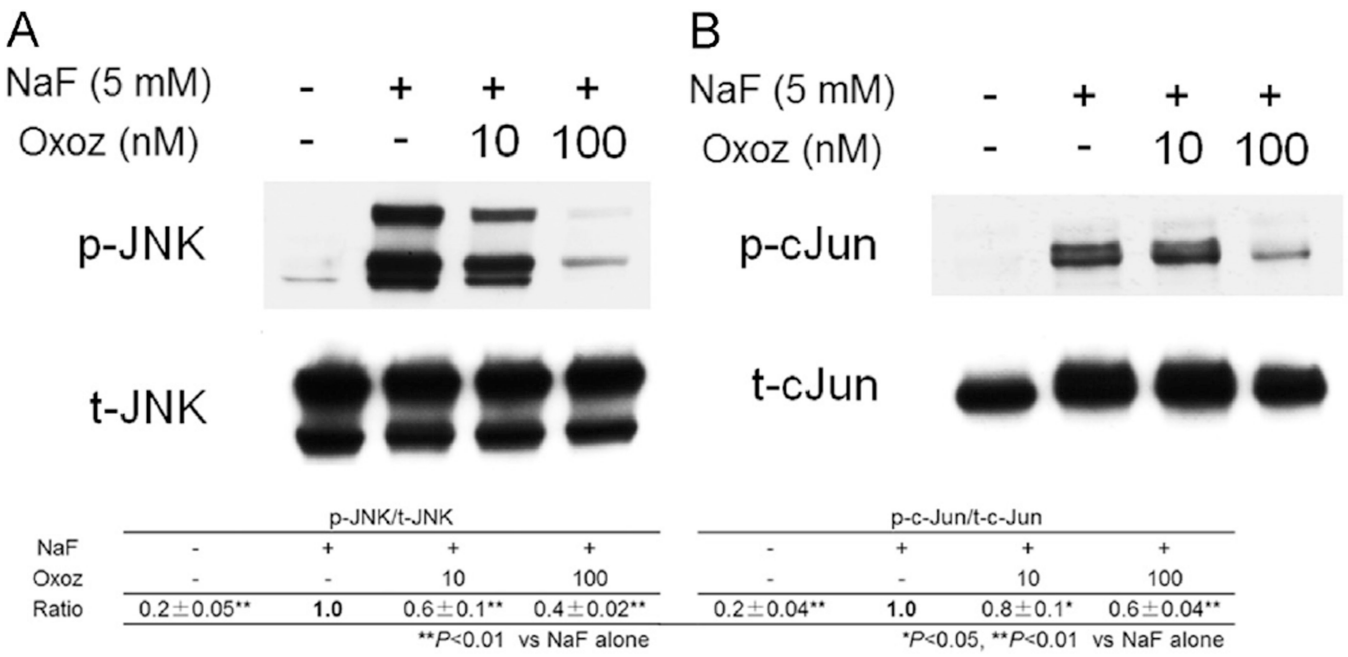

	p-JNK/t-JNK				p-c-Jun/t-c-Jun			
NaF	-	+	+	+	-	+	+	+
Oxoz	-	-	10	100	-	-	10	100
Ratio	0.2±0.05**	**1.0**	0.6±0.1**	0.4±0.02**	0.2±0.04**	**1.0**	0.8±0.1*	0.6±0.04**
			**P<0.01 vs NaF alone				*P<0.05, **P<0.01 vs NaF alone	

Fig. 4.

Fluoride activates the MAPKKK pathway. LS8 cells were treated with 10 or 100 nM TAK1 (MAP3K7) inhibitor, oxoseaenol (Oxoz), for 1 h prior to 5 mM fluoride treatment for 2 h. (A) Total protein was extracted at 2 h and p-JNK (46, 54 kDa), t-JNK (46, 54 kDa), p-c-Jun (48 kDa), and t-c-Jun (48 kDa) were quantified by western blot procedures. The tables show the ratios p-JNK/t-JNK or p-c-Jun/t-c-Jun. *$P < 0.05$, **$p < 0.01$ vs. fluoride treatment alone. These results show that TAK1 inhibition attenuated fluoride-induced JNK phosphorylation.

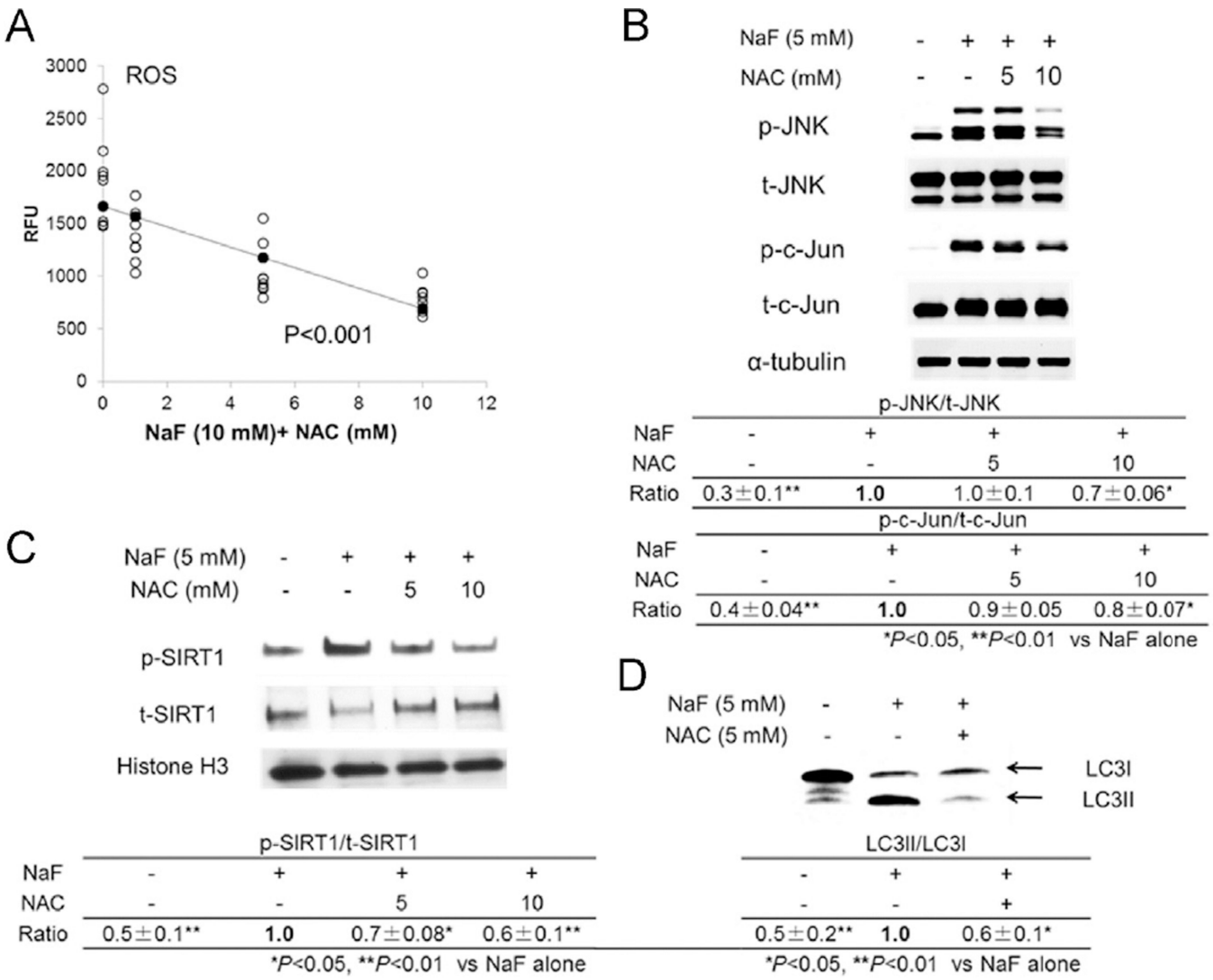

Fig. 5.

Fluoride activates SIRT1/autophagy through ROS-JNK signaling. LS8 cells were treated with 0, 5, or 10 mM N-acetylcysteine (NAC) for 1 h followed by 10 mM fluoride for 3 h. (A) Intracellular ROS generation was detected by H2DCFDA. Regression analysis revealed a highly significant negative correlation between NAC dose and ROS generation after fluoride treatment ($P < 0.001$). (B) Cells were treated with 5 or 10 mM NAC for 1 h followed by 5 mM fluoride for 2 h. p-JNK, t-JNK, p-c-Jun, and t-c-Jun were quantified by western blots. NAC treatment reduced p-JNK and p-c-Jun levels after fluoride exposure. α-tubulin (52 kDa) was the loading control protein. (C) Nuclear protein was extracted from cells treated with or without NAC (5 mM) pretreatment for 1 h followed by fluoride (5 mM) treatment for 6 h. p-SIRT1 and t-SIRT1 was quantified by western blots. At 6 h, NAC treatment decreased fluoride-induced p-SIRT1 levels. Histone H3 (17 kDa) was the loading control protein. (D) Cells were treated with 5 mM fluoride with or without 5 mM NAC for 24 h. Total protein was extracted and LC3I (16 kDa) and LC3II (14 kDa) were quantified by western blots. In the fluoride-treated samples, NAC reduced the levels of the autophagy

mediator LC3II. Tables show the ratios of p-JNK/t-JNK or p-c-Jun/t-c-Jun (B), p-SIRT1/t-SIRT1 (C), and LC3II/LC3I (D). *$P < 0.05$, **$p < 0.01$ vs. fluoride treatment alone.

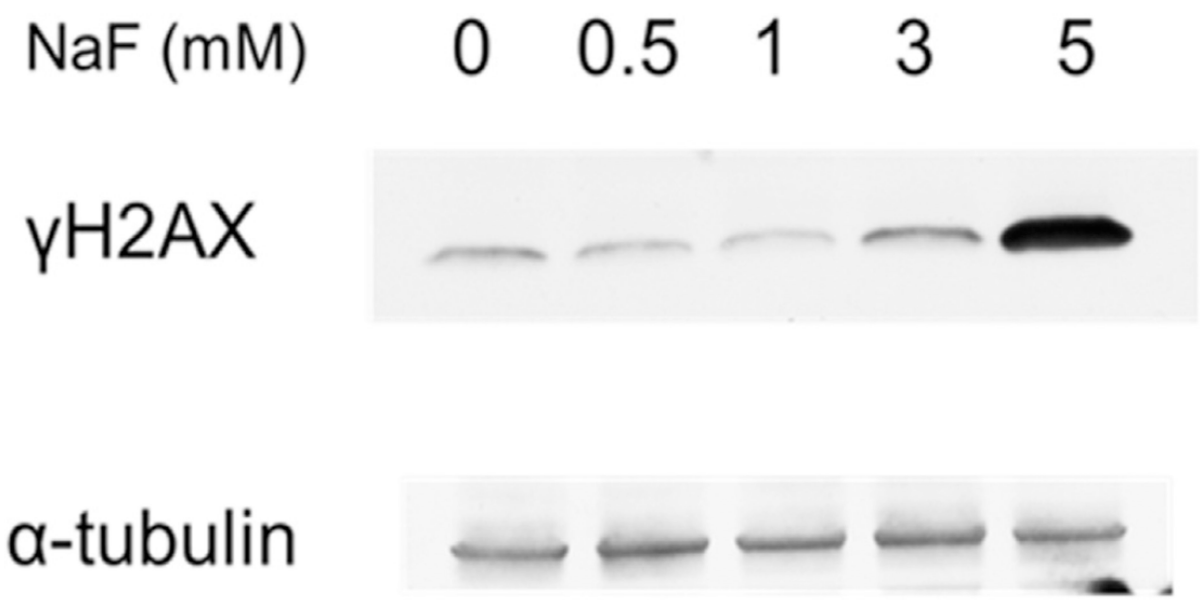

γH2AX/αTubulin

NaF	0 mM	0.5 mM	1 mM	3 mM	5 mM
Ratio	**1.0**	1.4 ± 0.03	2.2 ± 0.8	2.5 ± 0.9	3.5 ± 1.0

P<0.01 regression analysis

Fig. 6.

Fluoride induces DNA damage. LS8 cells were treated with 0–5 mM fluoride for 6 h. Total protein was extracted and the DNA double-strand break marker phosphorylated H2AX (γH2AX, 15 kDa) was quantified by western blots. Fluoride treatment at 3 and 5 mM increased the level of γH2AX. α-Tubulin was the loading control protein. The table shows the γH2AX/α-tubulin ratio. Regression analysis revealed a highly significant positive correlation between fluoride dose and γH2AX expression ($P < 0.01$).

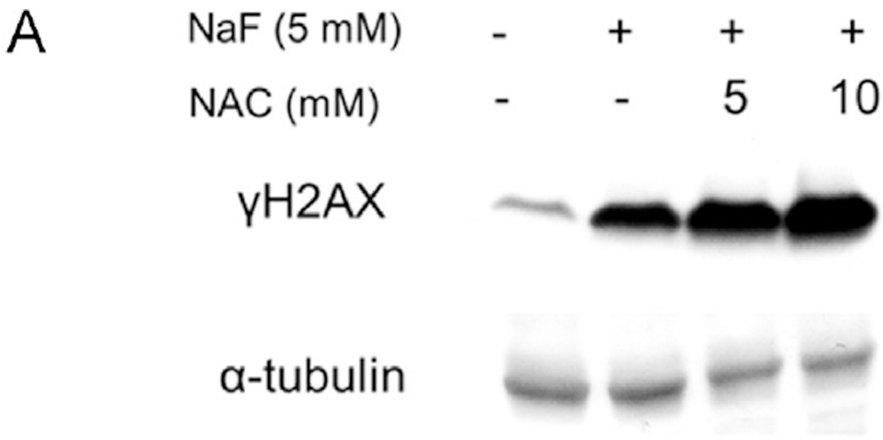

γH2AX/α-tubulin				
NaF	-	+	+	+
NAC	-	-	5	10
Ratio	0.3 ± 0.1**	**1.0**	1.5 ± 0.2	2.0 ± 0.6*

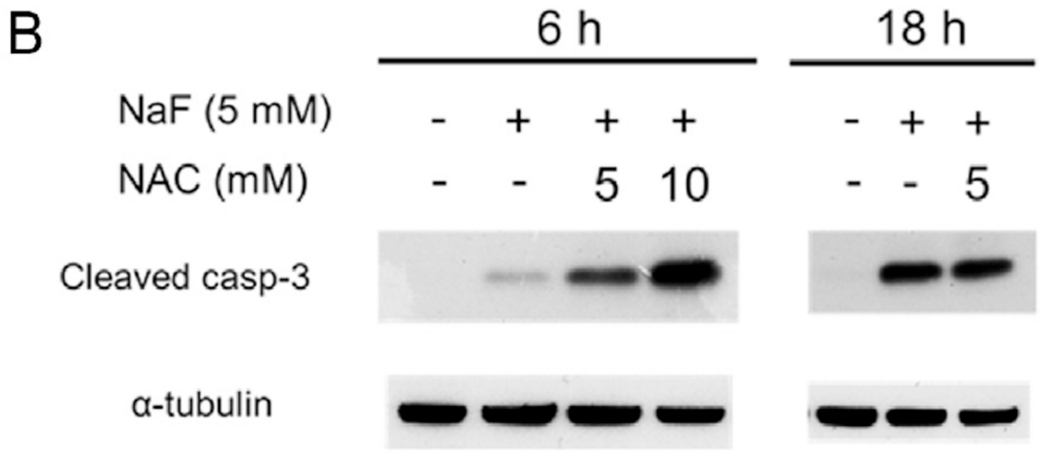

Cleaved-Cas3/α-tubulin							
	6 h				18 h		
NaF	-	+	+	+	-	+	+
NAC	-	-	5	10	-	-	5
Ratio	0.6 ± 0.1	**1.0**	1.6 ± 0.3	2.4 ± 0.7**	0.2 ± 0.07**	**1.0**	0.9 ± 0.2

Fig. 7.

NAC treatment increases the levels of fluoride-induced γH2AX and cleaved caspase-3. (A) LS8 cells were treated with or without 5 or 10 mM NAC for 1 h prior to 0 or 5 mM fluoride treatment for 6 h. Total protein was extracted and γH2AX was quantified by western blot analysis. NAC treatment significantly increased the amount of fluoride-induced γH2AX. (B) Cleaved-caspase-3 (17 kDa) was also quantified by western blots after treatment with 0, 5, or 10 mM NAC and 0 or 5 mM fluoride for 6 or 18 h. NAC treatment increased the levels of fluoride-induced cleaved caspace-3 at 6 h, but no significant difference was observed at 18

h. α-Tubulin was the loading control protein. Tables show the ratios of γH2AX/α-tubulin (A) or Cleaved-caspase-3/α-tubulin (B). *$P < 0.05$, **$p < 0.01$ vs. fluoride treatment alone.

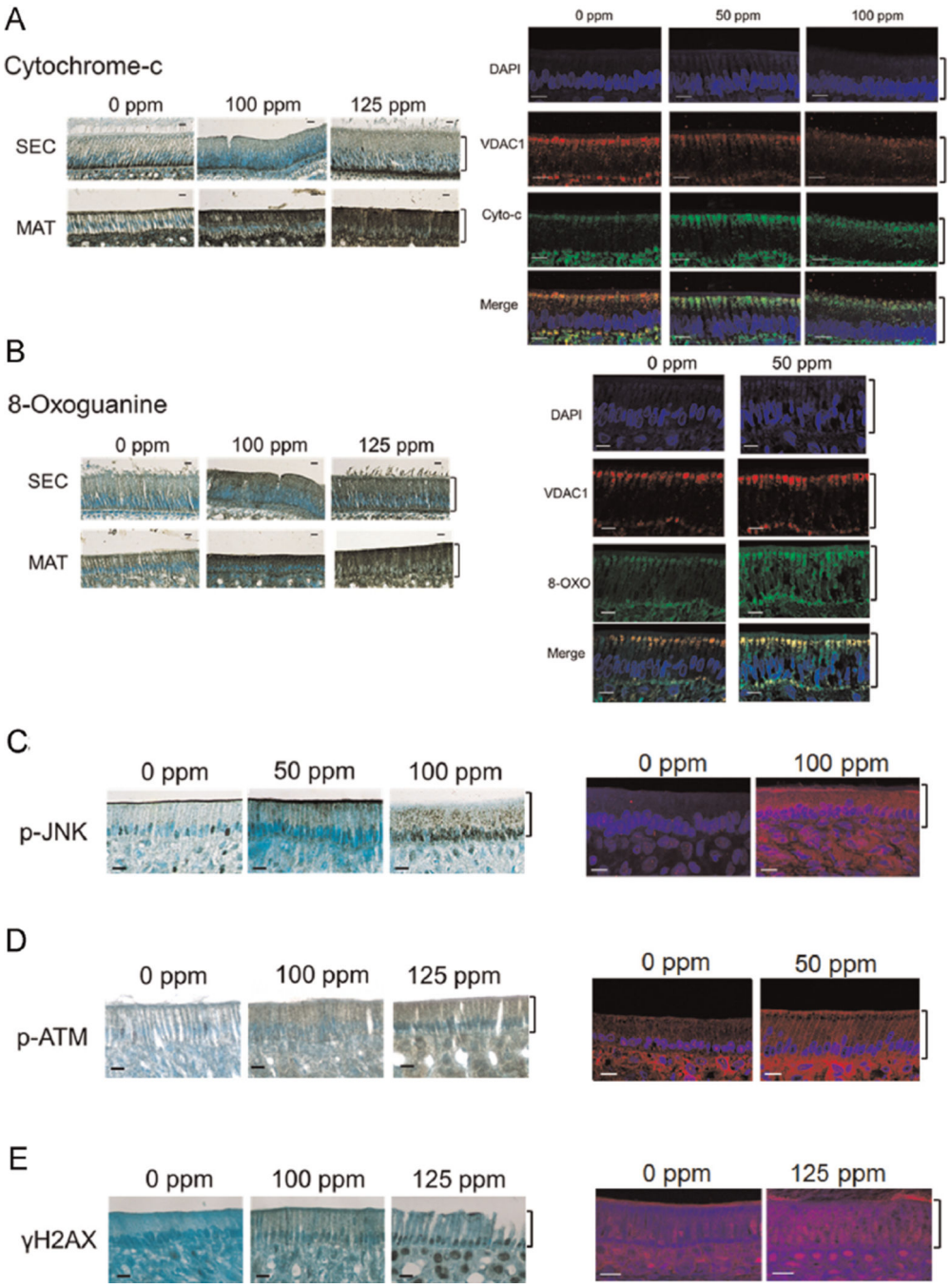

Fig. 8.

Fluoride-induced mitochondrial and DNA damage in rodent enamel organs. Rodents were provided water ad libitum containing 0, 50, 100, or 125 ppm fluoride as sodium fluoride for 6 weeks. Left panels show immunohistochemical (IHC) staining performed on paraffin sections from rat incisors in the secretory (SEC) or maturation (MAT) stage of enamel development. Right panels show immunofluorescent staining (IF) performed on paraffin sections from rat (A–D) or mouse (E) maturation-stage incisors. (A) Identification of cytochrome-c released into the ameloblast cytoplasm. Right panels show maturation-stage

enamel organs stained with DAPI to locate cell nuclei (blue), the mitochondria marker VDAC1 (red), and cytochrome-c (Cyto-c) stained green. Note that fluoride treatment caused release of cytochrome-c during the maturation stage of enamel development. (B) Identification of 8-oxoguanine in enamel organs stained with DAPI, VDAC1, or 8-oxoguanine (8-OXO). 8-Oxoguanine located primarily outside the nucleus in fluoride-treated secretory and maturation stage incisors. (C–E) Maturation-stage incisors stained with DAPI and phospho-(p)-JNK (C), phospho-(p)-ATM (D), or histone γH2AX (E). p-JNK, p-ATM, and γH2AX staining increased in fluoride-treated maturation stage ameloblasts in a dose-dependent manner. Scale bar represents 10 μm. Brackets denote ameloblasts.

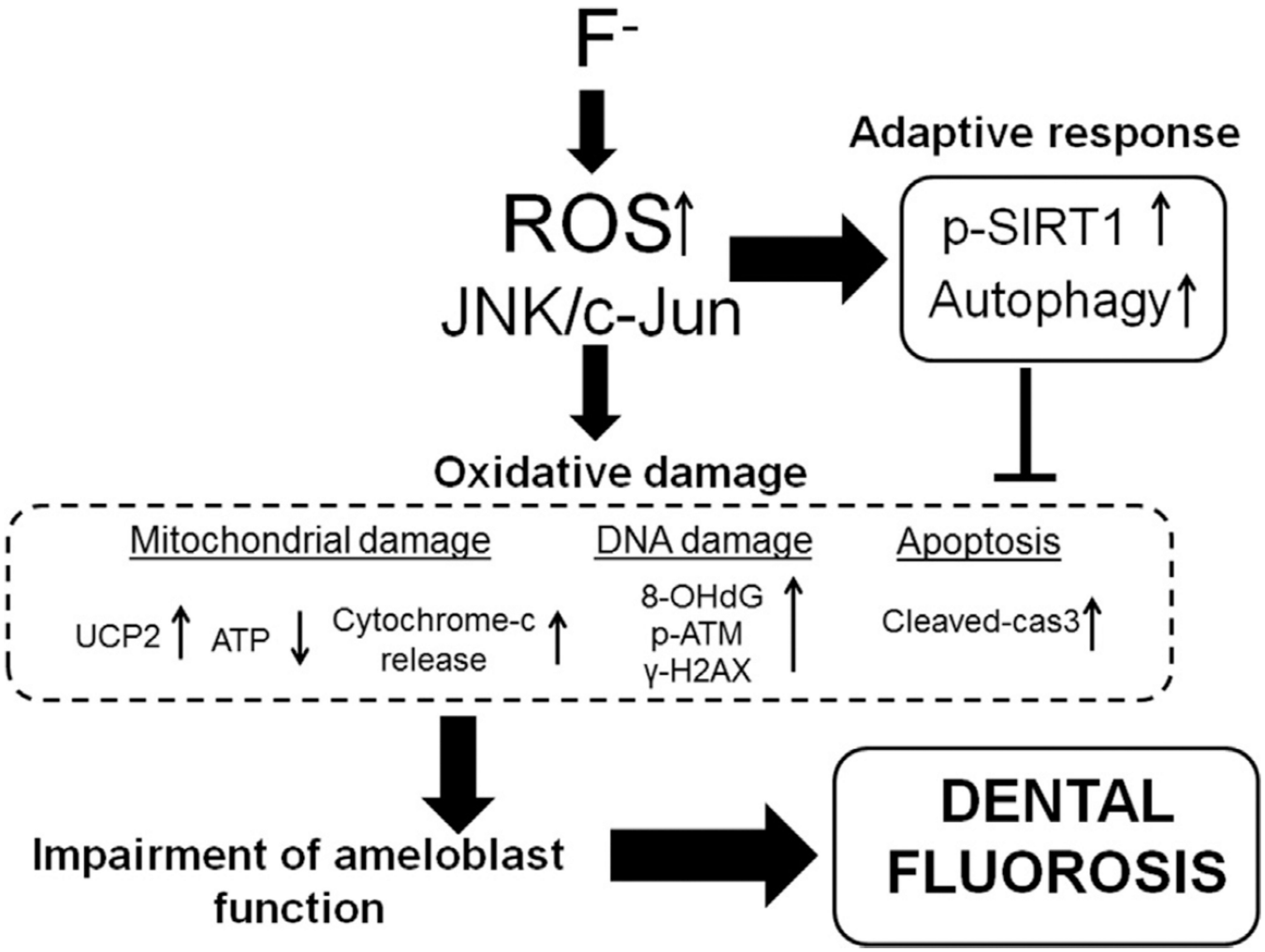

Fig. 9.

Schematic summary depicting fluoride-induced oxidative damage and adaptive response. Fluoride induces ROS generation that elicits JNK/c-Jun signaling. The ROS-mediated JNK/c-Jun pathway induces oxidative damage, mitochondrial damage, DNA damage, and apoptosis. Conversely, fluoride activates SIRT1/autophagy as an adaptive response through the ROS-mediated JNK/c-Jun pathway to protect cells from fluoride-induced oxidative damage.